moment at the transmitter, as well as function as detectors of the vector electric field at the receiver. As for the magnetic polarization components, we assume that three more resonant antenna structures, perhaps mutually orthogonal magnetic-sensing 'loops', could be designed to be collocated with the three orthogonal (electric-sensing) sleeves. Although the engineering details associated with magnetic-sensing antennae differ from those of electric-sensing ones, these differences have been successfully dealt with before[12,13].

Having constructed two such tri-polarized antennae, demonstrating their potential for increased capacity in a particular environment involves measuring the rank of the 3×3 electric transfer matrix H (that is, equation (1)) where contributions from **B** and **m** are ignored). A variety of pilot signals may be used to measure the transfer matrix H, but we chose simple sinusoids (tones) for purposes of characterization. Let α and β each denote one of the three indices of the transmit and receive antennae polarizations. The experimental procedure was to choose three distinct tones ω_β within a narrow frequency band (experimentally, it is found that H (equation (1)) varies negligibly over bands of 20 kHz) and transmit each on its own antenna element. All three frequencies were then observed on each of the three antenna elements at the receiver. The transfer matrix element $H_{\alpha\beta}$ could then be read off as the complex amplitude at frequency ω_β (transmitted on antenna β) received on antenna α.

The results are illustrated in the graph of Fig. 4, and show capacities inferred from the measured matrices. The upper curve is the "tripole" capacity (3×3 matrix), whereas the lower and middle curves are for 1×1 (scalar) and 2×2 (dual-polarized) submatrices, respectively. In the scalar and dual-polarized cases we present capacities averaged over the nine possible choices for antennae at the transmitter and receiver. (There are three possible ways of choosing either one or two antennae from three, and combinations of transmit and receive elements yields 3×3 or nine possibilities.) It is clear from the figure that use of polarization adds to the capacity, and does so in agreement with theory[6]. These data were taken in a large cafeteria (about 500 m^2, with 10-m high ceilings) with the transmitter and receiver around a corner from one another; each matrix was measured with the receiver at a different position but always about 25 m from the transmitter.

In order to provide an illustrative visual example of the expansion of channel capacity, we wirelessly communicated a colour image with colour represented as usual by a three-dimensional vector of red, green and blue components. These three monochrome image components of the original full-colour image were transmitted separately by each of the three transmit antennae, along with pilot signals allowing for measurement of the 3×3 transfer matrix H. The inset of Fig. 4 shows the recovered image (Joan Miro, *A toute épreuve*).

From these studies it is clear that electromagnetic polarization can play an important role in wireless communication. We have demonstrated experimentally the capacity increase that comes from exploiting the three-dimensional electric field vector (Fig. 4), and have theoretically shown the benefit arising from the use of magnetic degrees of freedom as well (Fig. 2). There will undoubtedly be practical issues to be considered in using a sixfold polarized antennae system, including the efficiency and cross-coupling of antennae extracting all the electromagnetic degrees of freedom near a point, as well as issues such as the statistics and environmental fluctuations that affect H. Nevertheless, the capacity increase is real and necessitates a re-evaluation of the use of polarization in wireless communication using electromagnetic waves. □

Received 4 July; accepted 26 October 2000.

1. Andrews, E. L. $50 billion for German wireless licenses. *The New York Times* 18 August (2000).
2. Jackson, J. D. *Classical Electrodynamics* (John Wiley, New York, 1975).
3. Singer, A. Space vs. polarization diversity. *Wireless Rev.* **15,** 164–166 (1998).
4. Winters, J. H. On the capacity of radio communication systems with diversity in a rayleigh fading environment. *IEEE J. Selected Areas Commun.* Vol. SAC-5, 871–878 (1987).
5. Foschini, G. J. & Gans, M. J. On limits of wireless communications in a fading environment when using multiple antennas. *Wireless Pers. Commun.* **6,** 311–335 (1998).
6. Telatar, I. E. Capacity of multi-antenna gaussian channels. *Eur. Trans. Telecommun.* **10,** 585–595 (1999).
7. Moustakas, A. L., Baranger, H. U., Balents, L., Sengupta, A. M. & Simon, S. Communication through a diffusive medium: Coherence and capacity. *Science* **287,** 287–290 (2000).
8. deCarvalho, R., Mitra, P. P. & Andrews, M. R. in *National Radio Science Meeting* 84 (International Union of Radio Science, National Academy of Sciences, 2000).
9. Morgan, M. & Evans, W. Synthesis and analysis of elliptic polarization loci in terms of space-quadrature sinusoidal components. *Proc. IRE* **39,** 552–556 (1951).
10. Hatke, G. F. in *Twenty-seventh Asilomar Conference on Signals, Systems & Computers* 1365–1369 (IEEE Computer Society Press, Los Alamitos, California, 1993).
11. Afraimovich, E. L., Chernukhov, V. V., Kobzar, V. A. & Palamartchouk, K. S. Determining polarization parameters and angles of arrival of hf radio signals using three mutually orthogonal antennas. *Radio Sci.* **34,** 1217–1225 (1999).
12. Kraus, J. D. *Antennas* 2nd edn 725–726 (McGraw Hill, Boston, 1988).
13. Lee, W. C. Y. Theoretical and experimental study of the properties of the signal from an energy-density mobile-radio antenna. *IEEE Trans.* **1,** 25–32 (1967).

Acknowledgements

This work is supported by internal funding at Bell Labs, Lucent Technologies. We are grateful to W. M. MacDonald for his assistance in characterizing our antenna's radiation patterns, and to M. J. Gans for his insights and discussions concerning magnetic polarization.

Correspondence and requests for materials should be addressed to M.R.A. (e-mail: mikea@bell-labs.com).

Relationship between structural order and the anomalies of liquid water

Jeffrey R. Errington & Pablo G. Debenedetti

Department of Chemical Engineering, Princeton University, Princeton, New Jersey 08544-5263, USA

In contrast to crystalline solids—for which a precise framework exists for describing structure[1]—quantifying structural order in liquids and glasses has proved more difficult because even though such systems possess short-range order, they lack long-range crystalline order. Some progress has been made using model systems of hard spheres[2,3], but it remains difficult to describe accurately liquids such as water, where directional attractions (hydrogen bonds) combine with short-range repulsions to

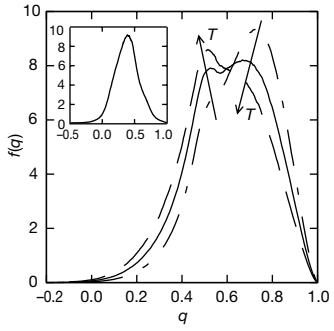

Figure 1 The effect of temperature on the distribution of the orientational order, q, at a density $\rho = 1.2$ g cm^{-3}. Three temperatures T are considered; 320 K (dashed line), 280 K (solid line) and 240 K (dot-dashed line). The fraction of molecules with q-values between $q + dq/2$ and $q - dq/2$ is $f(q)dq$. The area under each curve is normalized to unity. Arrows indicate the effect of increasing temperature. The possible range of q for a molecule is $-3 \leq q \leq 1$; the average value for a collection of molecules spans the range $0 \leq \langle q \rangle \leq 1$. Inset, the q-distribution for a Lennard–Jones system at a density $\rho^* = N\sigma^3/V = 1.0$ and temperature $T^* = k_B T/\epsilon = 2.0$, where ϵ and σ are the energy and size parameters, and k_B is Boltzmann's constant. For the Lennard–Jones fluid, $f(q)$ is virtually unchanged throughout the liquid region of the phase diagram.

determine the relative orientation of neighbouring molecules as well as their instantaneous separation. This difficulty is particularly relevant when discussing the anomalous kinetic and thermodynamic properties of water, which have long been interpreted qualitatively in terms of underlying structural causes. Here we attempt to gain a quantitative understanding of these structure–property relationships through the study of translational[2,3] and orientational[4] order in a model[5] of water. Using molecular dynamics simulations, we identify a structurally anomalous region—bounded by loci of maximum orientational order (at low densities) and minimum translational order (at high densities)—in which order decreases on compression, and where orientational and translational order are strongly coupled. This region encloses the entire range of temperatures and densities for which the anomalous diffusivity[6–9] and thermal expansion coefficient[10] of water are observed, and enables us to quantify the degree of structural order needed for these anomalies to occur. We also find that these structural, kinetic and thermodynamic anomalies constitute a cascade: they occur consecutively as the degree of order is increased.

We introduce two measures of order in water[11–14]. The translational order parameter[3] t measures the tendency of pairs of molecules to adopt preferential separations (see Methods). It vanishes for an ideal gas, and is large for a crystal. The orientational order parameter[4] q measures the extent to which a molecule and its four nearest neighbours adopt a tetrahedral arrangement[15], such as exists in hexagonal ice (I_h) (see Methods). It vanishes for an ideal gas, and equals 1 in a perfectly tetrahedral arrangement. Figure 1 shows the calculated distribution of q-values at different temperatures and fixed density (see Methods for details of the molecular dynamics simulations). The bimodal distribution suggests that the transient arrangement[14,16,17] adopted by a molecule and its four nearest neighbours can be described as being predominantly structured and 'ice'-like (high-q peak) or unstructured (low-q peak)[18,19]. This should not be interpreted as implying the existence of two fixed types of energetically favoured arrangements.

Figure 2 shows the calculated evolution of t and q on compression. At 260 K, starting from $\rho = 0.85\ \mathrm{g\,cm^{-3}}$, both t and q increase with density. At point A, water attains the maximum orientational order, and the hydrogen-bond network is at its most structured. Further compression leads to a decrease in q. Translational order is strongly coupled to orientational order under these conditions, causing t also to decrease upon compression. This means that hydrogen-bonding determines both the mutual orientation and the separation between molecules. Increasing the temperature weakens the coupling between translational and orientational order, and the decrease in q upon compression does not cause a corresponding decrease in t (400 K isotherm). A maximum in orientational order is attained at point C in Fig. 2. At this temperature, however, compression always causes translational order to increase, as in the hard-sphere liquid[2,3].

In order to investigate the relationship between molecular order and dynamics, we show in Fig. 3 the calculated dependence of the diffusion coefficient D upon density and temperature. Diffusivity maxima in water are well-documented experimentally[7,8] and by computer simulation[9]. Diffusivity minima have been reported only in simulations[6]. The anomalous region where $\mathrm{d}D/\mathrm{d}\rho$ is greater than zero disappears above 300 K. Figure 4 shows the calculated loci of diffusivity minima, diffusivity maxima, q maxima (for example, point A in Fig. 2), t minima (for example, point B in Fig. 2), and density maxima[20] (also known as temperature of maximum density or TMD[21]). Along the TMD locus, water's thermal expansion coefficient vanishes, and inside the region it encloses, the thermal expansion coefficient is negative. At low temperatures, the locus of maximum orientational order is very close to the locus of minimum diffusivity, with the 'closeness' becoming more pronounced the lower the temperature; at the lowest temperature studied, these loci

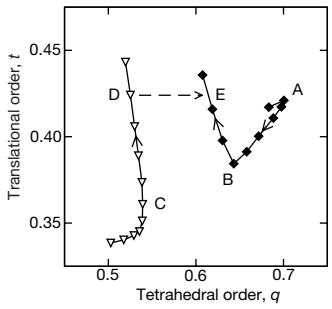

Figure 2 The path traversed in order-parameter space as liquid water is compressed isothermally at two different temperatures. Filled diamonds, $T = 260$ K; open triangles, $T = 400$ K. The arrows indicate the direction of increasing density, which varies from 0.85 to 1.3 g cm^{-3} ($T = 260$ K) and from 0.8 to 1.3 g cm^{-3} ($T = 400$ K), each symbol representing an increment of 0.05 g cm^{-3}. A and C are states of maximum orientational order at the respective temperatures. B is a state of minimum translational order. Along path D–E, t and q are independently variable, as one of them varies while the other is kept fixed.

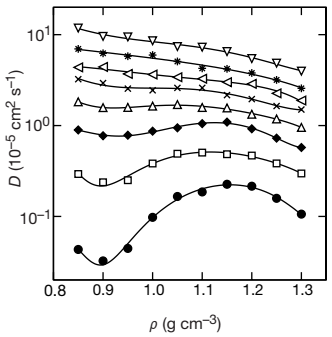

Figure 3 Density dependence of the diffusion coefficient, D, shown for eight isotherms. The curves from top to bottom correspond to temperatures T (in K) of: 400, 350, 320, 300, 280, 260, 240 and 220. The solid lines are fifth-order polynomial fits to the data, and are simply guides to the eye. The diffusion coefficient was calculated from the long-time behaviour of the mean squared displacement of the water molecules, $\langle r^2(t)\rangle$, using the Einstein relationship $6D = \mathrm{d}\langle r^2(t)\rangle/\mathrm{d}t$.

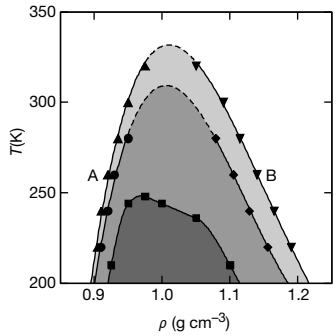

Figure 4 Relationship between loci of structural, dynamic and thermodynamic anomalies. The structurally anomalous region is bounded by the loci of q maxima (upward-pointing triangles) and t minima (downward-pointing triangles). Inside this region, water becomes more disordered when compressed, as t and q decrease with increasing density. The loci of diffusivity minima (circles) and maxima (diamonds) define the region of diffusive anomalies, where D increases with density. The thermodynamically anomalous region is defined by the TMD (squares), inside which the density increases when water is heated at constant pressure. We refer to the low-density boundary of the structurally anomalous region as a q-maximum locus, with the understanding that this applies to points such as A, which are maxima in q at which t decreases with increasing density, but not to C (Fig. 2), which lies outside the structurally anomalous region and for which the q maximum is not accompanied by a decrease in t.

are virtually within numerical error of each other. The locus of minimum translational order parallels the locus of diffusivity maxima. The TMD, and hence all states where the thermal expansion coefficient is negative, lies entirely inside the region defined by the loci of maximum q and minimum t. We refer to the region bounded by t and q extrema as structurally anomalous, because inside it orientational and translational order decrease by compression.

If the order parameters of states inside the structurally anomalous region are plotted in the (t, q) plane, we obtain, within the numerical accuracy of the simulations, a single line (Fig. 5). States outside the structurally anomalous region map onto the region of the (t, q) plane lying above this line. Therefore, all structurally anomalous states have the important property that their orientational and translational order are not independent, there being no thermodynamic path along which one can be varied while keeping the other fixed. Alternative scenarios, such as each isotherm being tangent at one point to—or coinciding over a limited range with—a common (t, q) envelope, cannot be ruled out within the numerical precision of the data. Outside the structurally anomalous region orientational and translational order are independently variable, as there exist paths along which one can be varied while the other is kept fixed, such as D–E (Fig. 2.) States inside the structurally anomalous region possess the maximum orientational order consistent with their translational order. Over the range of temperatures and densities investigated, we found no states lying below the line shown in Fig. 5.

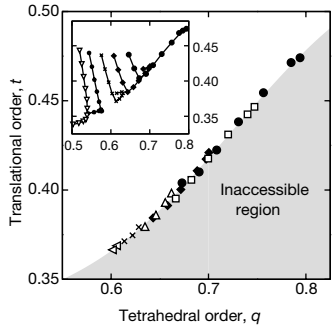

Figure 5 The line of structural anomalies in order-parameter space. The data points in the main panel correspond to state points that lie between the maximum in orientational order and the minimum in translational order along an isotherm, for example state points between A and B in Fig. 2. All state points within the structurally anomalous region bounded by triangles in Fig. 4 map onto the line shown in the main panel. Symbols for different temperatures are as in Fig. 3. Inset, five isotherms in order-parameter space that span the density range $0.85 \leq \rho \leq 1.3\ \mathrm{g\,cm^{-3}}$ (0.8 to $1.3\ \mathrm{g\,cm^{-3}}$ at 400 K). The data points in the main panel represent a subset of the points displayed in the inset. This subset corresponds to thermodynamic states inside the structurally anomalous region.

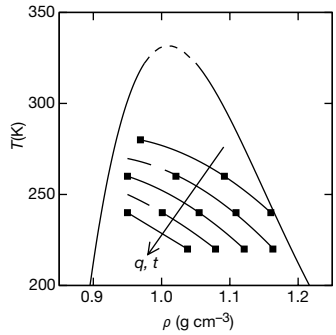

Figure 6 Isotaxis lines in the (T, ρ) plane. The q-difference between lines is constant ($\Delta q = 0.02$). The arrow indicates the direction of increasing order. The (q, t) values along the isotaxes (top to bottom) are (0.66, 0.394), (0.68, 0.405), (0.70, 0.417), (0.72, 0.429) and (0.74, 0.442). The outer solid and dashed lines define the structurally anomalous region. Lines through squares are guides to the eye. The slope of isentropic lines (not shown) has the same sign as the thermal expansion coefficient. Inside the TMD, therefore, isentropes and isotaxes have negative slope. Inside the structurally anomalous region but outside the TMD, isentropes have positive slope while isotaxes have negative slope: t and q do not possess the same information content as the entropy. It is not clear how much of the missing information is related to vibrational degrees of freedom or to higher-order correlations not included in t and q.

Because the line on the (t, q) plane onto which all structurally anomalous states are mapped has positive slope, it is possible to rank all such equilibrium states according to their relative order. This is done in Fig. 6, where several lines of constant t and q are shown. We call these isotaxis lines (from the Greek word *taxis*, meaning order, or arrangement). The isotaxis lines have negative slope in the (T, ρ) plane, with t and q jointly increasing in the direction of decreasing T and ρ. This reflects the fact that water becomes more structured upon cooling and expansion.

The physical picture that emerges from this work is the following. In liquid water there occurs a cascade of anomalies. Structural anomalies, whereby order decreases upon compression, occur over the broadest range of densities and temperatures. Diffusive anomalies, whereby D increases by compression, occur entirely inside the region of structural anomalies. Thermodynamic anomalies, whereby the density decreases upon cooling at constant pressure, occur entirely inside the region of diffusive anomalies. All anomalous states share the topological property that orientational and translational order are strongly coupled. Isotaxis lines rank thermodynamic states according to order. To each boundary of anomalies there corresponds a limiting tangent isotax that defines the minimum order needed for that anomaly to occur. For SPC/E water we find $q > 0.615$ for diffusive anomalies, and $q > 0.705$ for density anomalies.

As water's loci of diffusivity maxima and configurational entropy maxima coincide[9], future investigations could usefully determine whether the loci of diffusivity minima and configurational entropy minima also correspond. This would clarify the relationship between configurational entropy[22–24] and the structural indicators of anomalies introduced here. Liquid water possesses additional anomalies[10,25] not discussed here—for example, increase in the isothermal compressibility[26] and isobaric heat capacity[27,28] upon cooling, decrease in viscosity upon compression[29], a polyamorphic transition[10,19,21,25] and the possible existence of a second critical point[10,21,25,30]. Another area for future work would be the determination of the structural limits where each component in the cascade of anomalies occurs. Our results suggest that the quantification of order may offer new insights into the properties of liquids, glasses and other condensed-phase systems. □

Methods

Order parameters

The translational order parameter t is given by[3]

$$t = \frac{\int_0^{\xi_c} |g(\xi) - 1| \mathrm{d}\xi}{\xi_c}$$

where ξ ($= r\rho^{1/3}$) is the distance between the oxygen atoms of a pair of molecules, r, divided by the mean separation between a pair of molecules at the given density, $\rho^{-1/3}$; ρ denotes the density, or number of molecules per unit volume (N/V); g is the oxygen–oxygen radial distribution function; and ξ_c is a cut-off distance. We use $\xi_c = 2.843$ in this work. In an ideal gas, $g = 1$ and t vanishes. In a crystal, on the other hand, there is long-range translational order, and $g \neq 1$ over long distances. Hence t is large. Alternative definitions of translational order can be used when the underlying crystal structure is known[2,3]. However, the stable crystal form of the SPC/E model of water is not known. The basic features that define the relationship between translational order and density, and therefore between translational and orientational order, are insensitive to the precise definition of t (refs 2, 3). The orientational order parameter is given by

$$q = 1 - \frac{3}{8} \sum_{j=1}^{3} \sum_{k=j+1}^{4} \left(\cos\psi_{jk} + \frac{1}{3} \right)^2$$

where ψ_{jk} is the angle formed by the lines joining the oxygen atom of a given molecule and those of its nearest neighbours j and k (≤ 4). This definition is a rescaled version of the parameter introduced in ref. 4, in such a way that the average value of q varies between 0 (in an ideal gas) and 1 (in a perfect tetrahedral network). If a molecule is located at the centre of a regular tetrahedron whose vertices are occupied by its four nearest neighbours, $\cos\psi_{jk} = -1/3$. Thus, in a perfect tetrahedral network, $q = 1$. If, on the other hand, the mutual arrangement of molecules is random, as in an ideal gas, the six angles associated with the central molecule are independent, and the mean value of q vanishes:

$$\langle q \rangle = 1 - \frac{9}{8}\int_0^{\pi}\left(\cos\psi + \frac{1}{3}\right)^2 \sin\psi \mathrm{d}\psi = 0$$

Alternative measures of order can be used. They do not change the general picture shown in Fig. 4. We have tested the 'tetrahedrality parameter' of ref. 31 as an alternative measure of orientational order, and the two-body excess entropy of ref. 32 as an alternative measure of translational order[2]. Isotherms of these order parameters exhibit extrema with respect to density that are within 1.7% of those of q and t. The extrema loci define a structurally anomalous region almost identical to the one shown in Fig. 4. In particular, it lies entirely outside the region of diffusive anomalies, confirming that structural anomalies occur over the broadest range of densities and temperatures and anticipate the occurrence of transport and thermodynamic anomalies.

Molecular dynamics simulations

Our results are based on constant temperature and density molecular dynamics simulations[33] of 256 particles interacting via the shifted-force SPC/E potential[5] in a cubic box with periodic boundary conditions. The Ewald summation[33] was used to account for electrostatic interactions. The Lennard–Jones potential and real-space part of the Ewald summation were cut and linearly shifted to bring the energy and force to zero at a distance of 7.9 Å. The temperature was maintained using a Berendsen rescaling of the velocities with a relaxation time of 0.5 ps, and the equations of motion were solved using the velocity-Verlet and the RATTLE algorithm with a time step of 2 fs (ref. 33). For each of the densities examined, initial configurations were generated randomly and equilibrated using Monte Carlo techniques at the highest temperature considered in this study, 400 K. Molecular dynamics simulations were started using the final particle positions of a previous simulation at a state point as near as possible to the new one. Each system was equilibrated for between 0.5 and 15 ns, depending on the state point, followed by a production phase (of length greater than or equal to the equilibration phase), during which the properties of interest were sampled every 40 ps.

Location of diffusivity extrema

Isochores of the $T \leq 300$ K data were fitted to the power law $D(T) = D_0(T/T_0 - 1)^{\gamma}$, where D_0, T_0 and γ are density-dependent adjustable parameters. Subsequently, the diffusivity minima were located from spline fits to isotherms generated by the power-law functions, and the diffusivity maxima were obtained from fifth-order polynomial fits to the isotherms. The temperatures of maximum density (squares in Fig. 4) were obtained from fourth-order polynomial fits to isochores of pressure as a function of temperature. The positions of the extrema in orientational and translational order were extracted from spline fits to isotherms of the respective order parameter as a function of density.

Received 12 September; accepted 14 November 2000.

1. Ashcroft, N. W. & Mermin, N. D. *Solid State Physics* (Saunders College Publishing, Fort Worth, 1976).
2. Torquato, S., Truskett, T. M. & Debenedetti, P. G. Is random close packing of spheres well defined? *Phys. Rev. Lett.* **84,** 2064–2067 (2000).
3. Truskett, T. M., Torquato, S. & Debenedetti, P. G. Towards a quantification of disorder in materials. Distinguishing equilibrium and glassy sphere packings. *Phys. Rev. E* **62,** 993–1001 (2000).
4. Chau, P.-L. & Hardwick, A. J. A new order parameter for tetrahedral configurations. *Mol. Phys.* **93,** 511–518 (1998).
5. Berendsen, H. J. C., Grigera, R. J. & Stroatsma, T. P. The missing term in effective pair potentials. *J. Phys. Chem.* **91,** 6269–6271 (1987).
6. Ruocco, G., Sampoli, M., Torcini, A. & Vallauri, R. Molecular dynamics results for stretched water. *J. Chem. Phys.* **99,** 8095–8104 (1993).
7. Prielmeier, F. X., Lang, E. W., Speedy, R. J. & Lüdemann, H.-D. Diffusion in supercooled water to 300 MPa. *Phys. Rev. Lett.* **59,** 1128–1131 (1987).
8. Angell, C. A., Finch, E. D., Woolf, L. A. & Bach, P. Spin-echo diffusion coefficients of water to 2380 bar and −20 °C. *J. Chem. Phys.* **65,** 3063–3066 (1976).
9. Scala, A., Starr, F. W., La Nave, E., Sciortino, F. & Stanley, H. E. Configurational entropy and diffusivity of supercooled water. *Nature* **406,** 166–169 (2000).
10. Debenedetti, P. G. *Metastable Liquids. Concepts and Principles* (Princeton University Press, Princeton, 1996).
11. Tanaka, H. Simple physical explanation of the unusual thermodynamic behavior of liquid water. *Phys. Rev. Lett.* **80,** 5750–5753 (1998).
12. Tanaka, H. Two-order-parameter description of liquids: critical phenomena and phase separation in supercooled liquids. *J. Phys. Condens. Matter* **11,** L159–L168 (1999).
13. Tanaka, H. Simple physical model of liquid water. *J. Chem. Phys.* **112,** 799–809 (2000).
14. Shiratani, E. & Sasai, M. Molecular scale precursor of the liquid-liquid phase transition of water. *J. Chem. Phys.* **108,** 3264–3276 (1998).
15. Paschek, D. & Geiger, A. Simulation study on the diffusion motion in deeply supercooled water. *J. Phys. Chem. B* **103,** 4139–4146 (1999).
16. Sciortino, F., Poole, P. H., Stanley, H. E. & Havlin, S. Lifetime of the bond network and gel-like anomalies in supercooled water. *Phys. Rev. Lett.* **64,** 1686–1689 (1990).
17. Sciortino, F., Geiger, A. & Stanley, H. E. Effect of defects on molecular mobility in liquid water. *Nature* **354,** 218–221 (1991).
18. Soper, A. K. & Ricci, M. A. Structures of high-density and low-density water. *Phys. Rev. Lett.* **84,** 2881–2884 (2000).
19. Bellissent-Funel, M.-C. Is there a liquid-liquid phase transition in supercooled water? *Europhys. Lett.* **42,** 161–166 (1998).
20. Angell, C. A. & Kanno, H. Density maxima in high-pressure supercooled water and liquid silicon dioxide. *Science* **193,** 1121–1122 (1976).
21. Poole, P. H., Sciortino, F., Essman, U. & Stanley, H. E. Phase behavior of metastable water. *Nature* **360,** 324–328 (1992).
22. Sciortino, F., Kob, W. & Tartaglia, P. Inherent structure entropy of supercooled liquids. *Phys. Rev. Lett.* **83,** 3214–3217 (1999).
23. Stillinger, F. H. A topographic view of supercooled liquids and glass formation. *Science* **267,** 1935–1939 (1995).
24. Goldstein, M. Viscous liquids and the glass transition. A potential energy barrier picture. *J. Chem. Phys.* **51,** 3728–3739 (1969).
25. Mishima, O. & Stanley, H. E. The relationship between liquid, supercooled and glassy water. *Nature* **396,** 329–335 (1998).
26. Speedy, R. J. & Angell, C. A. Isothermal compressibility of supercooled water and evidence for a thermodynamic singularity at −45 °C. *J. Chem. Phys.* **65,** 851–858 (1976).
27. Angell, C. A., Oguni, M. & Sichina, W. J. Heat capacity of water at extremes of supercooling and superheating. *J. Phys. Chem.* **86,** 998–1002 (1982).
28. Tombari, E., Ferrari, C. & Salvetti, G. Heat capacity anomaly in a large sample of supercooled water. *Chem. Phys. Lett.* **300,** 749–751 (1999).
29. DeFries, T. & Jonas, J. Pressure dependence of NMR proton spin-lattice relaxation times and shear viscosity in liquid water in the temperature range −15 to 10 °C. *J. Chem. Phys.* **66,** 896–901 (1977).
30. Mishima, O. & Stanley, H. E. Decompression-induced melting of ice IV and the liquid–liquid transition in water. *Nature* **392,** 164–168 (1998).
31. Naberukhin, Y. I., Voloshin, V. P. & Medvedev, N. M. Geometrical analysis of the structure of simple liquids: percolation approach. *Mol. Phys.* **73,** 917–936 (1991).
32. Nettleton, R. E. & Green, M. S. Expression in terms of molecular distribution functions for the entropy density in an infinite system. *J. Chem. Phys.* **29,** 1365–1370 (1958).
33. Allen, M. P. & Tildesley, D. J. *Computer Simulation of Liquids* (Clarendon Press, Oxford, 1990).

Acknowledgements

We thank T.M. Truskett and S. Torquato for discussions. This work was supported by the US Department of Energy and Unilever Research.

Correspondence and requests for materials should be addressed to P.G.D. (e-mail: pdebene@princeton.edu).

Transparent nematic phase in a liquid-crystal-based microemulsion

Jun Yamamoto* & Hajime Tanaka

Institute of Industrial Science, University of Tokyo, 4-6-1 Komaba, Meguro-ku, Tokyo 153-8505, Japan

Complex fluids[1,2] are usually produced by mixing together several distinct components, the interactions between which can give rise to unusual optical and rheological properties of the system as a whole. For example, the properties of microemulsions (composed of water, oil and surfactants) are determined by the microscopic structural organization of the fluid that occurs owing to phase separation of the component elements. Here we investigate the effect of introducing an additional organizing factor into such a fluid system, by replacing the oil component of a conventional water-in-oil microemulsion with an intrinsically anisotropic fluid—a nematic liquid crystal. As with the conventional case, the fluid phase-separates into an emulsion of water microdroplets (stabilized by the surfactant as inverse micelles) dispersed in the 'oil' phase. But the properties are further influenced by a significant directional coupling between the liquid-crystal molecules and the surfactant tails that emerge (essentially radially) from the micelles. The result is a modified bulk-liquid crystal that is an ordered nematic at the mesoscopic level, but which does not exhibit the strong light scattering generally associated with bulk nematic order[2]: the bulk material here is essentially isotropic and thus transparent.

* Present address: Yokoyama Nano-structured Liquid-crystal Project, Tsukuba 300-2635, Japan.